



OPEN Symbiotic interactions on middle Cambrian echinoderms reveal the oldest parasitism on deuterostomes

Iban Goñi¹✉, Claude Monnet¹, Kenneth De Baets², Timothy P. Topper^{3,4}, Sylvie Régnier¹, Laurenz Schröer⁵, Veerle Cnudde^{5,6}, Peter A. Jell⁷ & Sébastien Clausen¹

Biotic interactions are considered as major drivers of evolutionary changes, but their identification in the fossil record is extremely rare and controversial. Based on qualitative and quantitative analyses, we report evidence of a biotic interaction between an echinoderm host and its symbiont, probably a parasitic epibiont, from the Cambrian Wuliuan Stage of Australia. The echinoderm plates bear external outgrowths with a median pit at their distal end. These unusual structures have not been previously documented from Cambrian echinoderms and their lack of consistency across various morphological parameters, supports the interpretation that a biotic interaction generated these unique structures. Perturbations in plate microstructure and the overproduction of skeletal material in specific regions, together with reduced size, negatively impact the host's growth suggesting a parasitic interaction. This reaction by the echinoderm host may represent the progressive embedment of the invasive epibiont. This record represents the oldest evidence of parasitism among deuterostomes.

The reconstruction of past ecosystems and their evolutionary history rely on the analyses of palaeobiodiversity, species interactions, biotic innovations, and species ecospace^{1–3}. Biotic interactions are essential elements of biological ecosystems. However, determining close symbiotic associations between two species, even when studying living organisms⁴, has proven to be an arduous task. Fossil associations providing direct evidence of biotic interactions, such as predation, are comparatively rare and mostly inferred from traces and functional morphology⁵. Symbiotic interactions between species, including commensalism, mutualism and parasitism, are crucial to reconstruct ecosystems but are difficult to interpret. This leads to a depreciation of symbiont biodiversity in the fossil record as well as a misunderstanding regarding their ecological or (co-)evolutionary role⁶. Another challenge in the fossil record, beyond identifying evidence of interactions, is determining the actual impact—whether positive, neutral, or negative—on the host and symbiont involved. Assessing these effects requires large sample sizes, which are often difficult to obtain from fossil assemblages⁷.

The first complex metazoan ecosystems are considered to have emerged during the Ediacaran–Cambrian transition (ca. 540 Ma), a time that also witnessed a dramatic increase in biotic interactions⁸. Biotic interactions already reported from the Cambrian include predation⁹, commensalism^{10,11}, competition¹² and parasitism^{13,14}. Parasitism is a long-term exploitative interaction between two organisms, where the interaction benefits the parasite and is detrimental to the host¹⁵. Possible parasitic infestations in the Cambrian are mainly reported as skeletal pathologies and calluses interpreted to be caused by parasites¹³, albeit their fossil record remains poor. This is despite the presence of numerous Cambrian Konservat-Lagerstätten^{16–19} that have provided an unparalleled view of the Cambrian seafloor through exceptional soft-bodied preservation. This perhaps not only highlights the difficulty in preserving biotic interactions but also possessing enough information to reliably interpret a parasitic relationship¹⁴. For example, the oldest confidently identified symbiont on deuterostomes – a major, disparate clade encompassing chordates (including vertebrates), hemichordates, and echinoderms – has

¹Univ. Lille, CNRS, UMR 8198 – Evo-Eco-Paleo, F-59000 Lille, France. ²Institute of Evolutionary Biology, Faculty of Biology, Biological and Chemical Research Centre, University of Warsaw, Warsaw, Poland. ³State Key Laboratory of Continental Dynamics, Shaanxi Key Laboratory of Early Life & Environments and Department of Geology, Northwest University, Xi'an 710069, China. ⁴Department of Palaeobiology, Swedish Museum of Natural History, Stockholm Box 50007, 10405, Sweden. ⁵PProGReSS-UGCT, Department of Geology, Ghent University, 9000 Ghent, Belgium. ⁶Environmental Hydrogeology, Department of Earth Sciences, Utrecht University, 3584 CB Utrecht, The Netherlands. ⁷School of Earth and Environmental Sciences, The University of Queensland, St Lucia, QLD 4072, Australia. ✉email: iban.goni@univ-lille.fr

been identified as a commensal relationship¹⁰. Other interactions have remained ambiguous²⁰. However, the echinoderm mesodermal skeleton has a high potential to preserve various types of parasitic interactions, and the record of biotic interaction with echinoderms through the Phanerozoic (Ordovician to present) has been well documented¹⁵. Here we report outgrowths on middle Cambrian echinoderm plates (Miaolingian Series, Wuliuan Stage) from the Georgina Basin, Australia that we interpret as resulting from the oldest symbiotic interaction, most probably parasitic, on deuterostome representatives.

Echinoderm disarticulated fragments, commonly referred to as plates or ossicles, were collected from middle Cambrian (Miaolingian Series, Wuliuan Stage) rocks of the Burke River Structural Belt, in the sedimentary sub-basin Duchess Embayment, in the eastern part of the Georgina Basin, Australia (Fig. 1). The calcareous sediments from the Beetle Creek Formation have yielded a rich and diverse fauna, largely echinoderm-dominated²¹. More than ten thousand phosphatized echinoderm plates were extracted, among which 120 display one or more external outgrowths. Outgrowths have only been recorded on echinoderm plates identified as epispire-bearing thecal plates (Figs. 2 and 3 and Supplementary Figs. 1 and 2). The theca is the main component of the echinoderm's skeleton that encapsulates most organs and epispire are notches on the plate margin that have been interpreted as respiratory structures. Epispire-bearing thecal plates are common among Cambrian echinoderm groups, preventing any precise unequivocal taxonomic identification of the specimens from Georgina Basin²². The non-infested and infested thecal plates and their outgrowths were studied comparatively by means of qualitative and quantitative approaches, including microstructure (stereom) description and development through Synchrotron and lab-based CT-scanning, quantification of their size and geometric properties, as well as their abundance and spatial distribution. All results indicate that the outgrowths are a result of a parasitic interaction. The abundance of infested echinoderm plates reported herein also confirms the polyphyletic setting of biotic interactions in early Cambrian ecosystems and offers a unique opportunity to shed light on parasitism of deuterostome animals as early as the middle Cambrian (ca. 509 Ma).

Results

Outgrowth morphology and microstructure

Outgrowths are cylindrical to dome-shaped structures with a variably developed distal median pit (20 to 70 μm in diameter; Fig. 2 and Supplementary Figs. 1 and 2). Outgrowths vary from 70 to 190 μm in diameter (Supplementary Fig. 3), and from 40 to 210 μm in height (Supplementary Fig. 4). Their diameter can be: (i) larger at the base than at the distal end (dome-shaped outgrowths, see Fig. 2d-f); (ii) quite constant all along the structure (cylindrical outgrowths, see Fig. 2c); and (iii) in rare cases, larger at the distal end than at the base (Fig. 2h). The diameter and the height of outgrowths follow a positive correlation (Supplementary Fig. 5), although variation remains important.

The outer stereom of the outgrowth is thinner and denser in comparison to the surrounding surface of the plate. Beside this surface observation, the exquisite preservation of the studied plates and associated outgrowths allows the detailed description of their stereom microstructure through CT-scanning. Different constructions (Fig. 3 and Supplementary Figs. 2 and 6) are observed among recovered plates, with 2 to 3 layers of different stereom fabric, coarseness, and density. The external surface of all scanned plates is made of a coarse, labyrinthic stereom delimiting large cylindrical galleries oriented perpendicular to the surface. This layer varies in thickness between plates but is relatively constant within a plate. The inner surface of the plates is invariably composed of a relatively dense labyrinthic stereom with limited variations in coarseness and density. A third, intermediate, thin layer of a more organized, somehow fascicular stereom layer is sometimes observed between the inner dense layer and the external coarse layer.

The outgrowth microstructure is relatively constant, whatever the morphology of the bearing plate, and consists of a dense labyrinthic stereom that tends to become somehow fascicular around a few well-developed median pits (in apparently most developed outgrowths, Supplementary Fig. 2h). In some outgrowths, a median, dense to unperforated stereom fills the basal part of the pit (Fig. 3h-i and Supplementary Fig. 2h), although post-sedimentary filling cannot be excluded. In cross-section (Fig. 3 and Supplementary Fig. 2), the median pits are most often superficial; but in some cases, the pit can be deeper and can even reach the base of the outgrowth (Fig. 2b). The microstructure of the plate is slightly to significantly perturbed below and around the outgrowth (Fig. 3 and Supplementary Figs. 2 and 6).

Outgrowths and relationship with plates

A diverse assemblage of about 20,000 echinoderm ossicles, including about 2000 epispire-bearing thecal plates, has been recovered from the Monastery Creek Phosphorite Member. Outgrowths are rare among this assemblage, being reported from only 120 epispire-bearing thecal plates (ca. 6%). Outgrowths exclusively develop on the external surface of the plates but independent of the plate morphology (see the morphospace analysis in Supplementary Fig. 7). Nevertheless, outgrowth bearing plates are reduced in size, being smaller than the uninfested ones, as shown by the analysis of their mean centroid size (Fig. 4a). However, there is no clear relationship between the size of a plate and the number of outgrowths it develops (Fig. 4b).

The number of outgrowths per plate varies from 1 to 5 (Supplementary Figs. 1 and 8), plates bearing one single outgrowth being the most common. Outgrowths are not evenly distributed on the surface of the plate (Supplementary Fig. 9). A single plate can display several outgrowths of different sizes, developed either close to the plate's margin, or close to its center, independently to the number of outgrowths present on the plate (Fig. 2i and Supplementary Fig. 1x). The development of the outgrowths variably initiates at different constitutive layers of the plates. Such variation is even observed between the microstructure of different outgrowths developed on the same plate. The outgrowths either develop (i) in continuation with the inner labyrinthic layer of the plates, surrounded by the external coarse stereom layer (Supplementary Fig. 6a); or (ii) within the external stereom

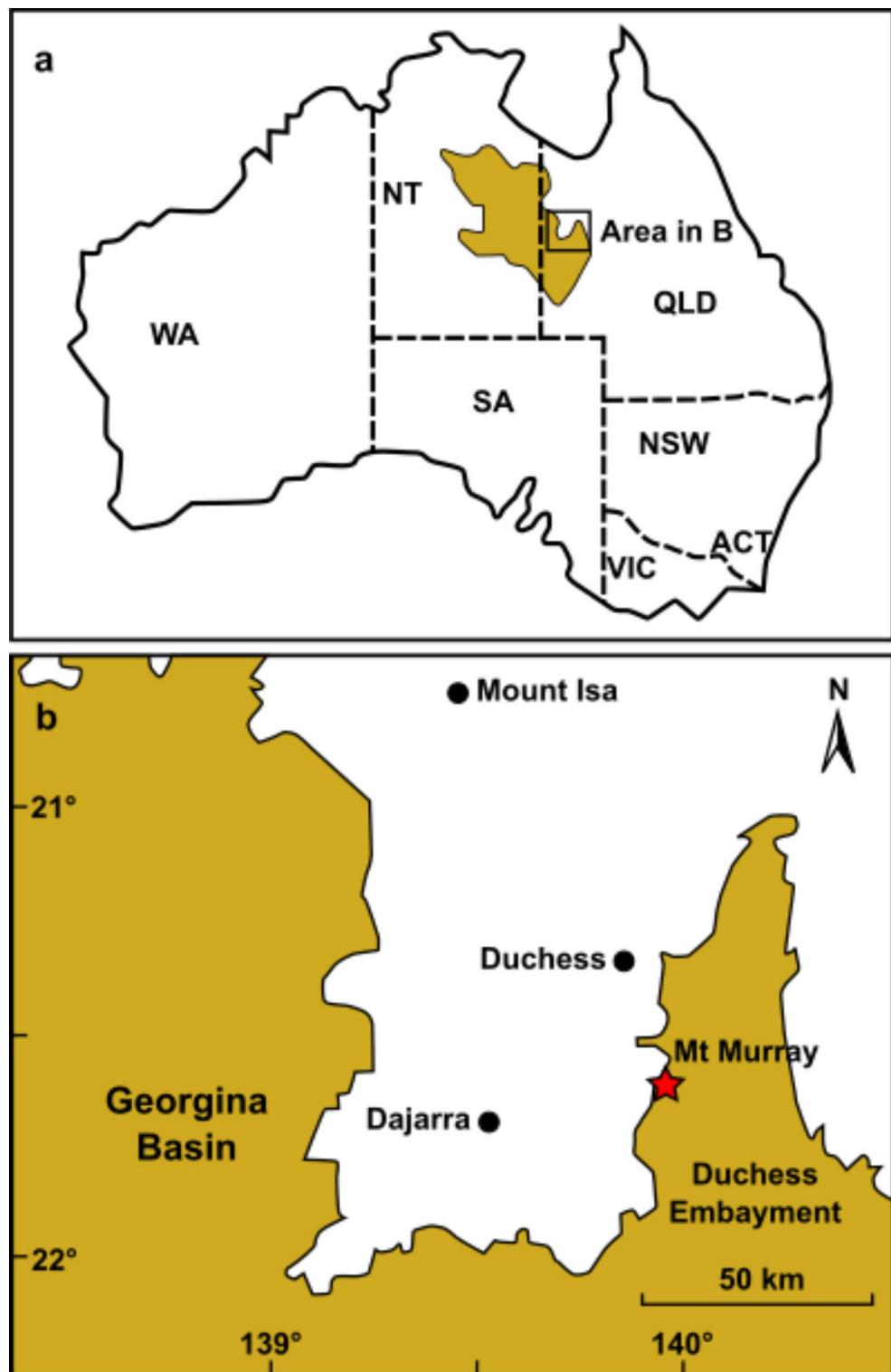


Fig. 1. Map of locality. (a) Map of Australia, highlighting the Georgina Basin (coloured). (b) Close-up on the study area; the fossiliferous locality in Mount Murray is marked by the red star (after Clausen et al.²⁵). WA = Western Australia; NT = Northern Territory; SA = South Australia; QLD = Queensland; NSW = New South Wales; ACT = Australian Capital Territory; VIC = Victoria.

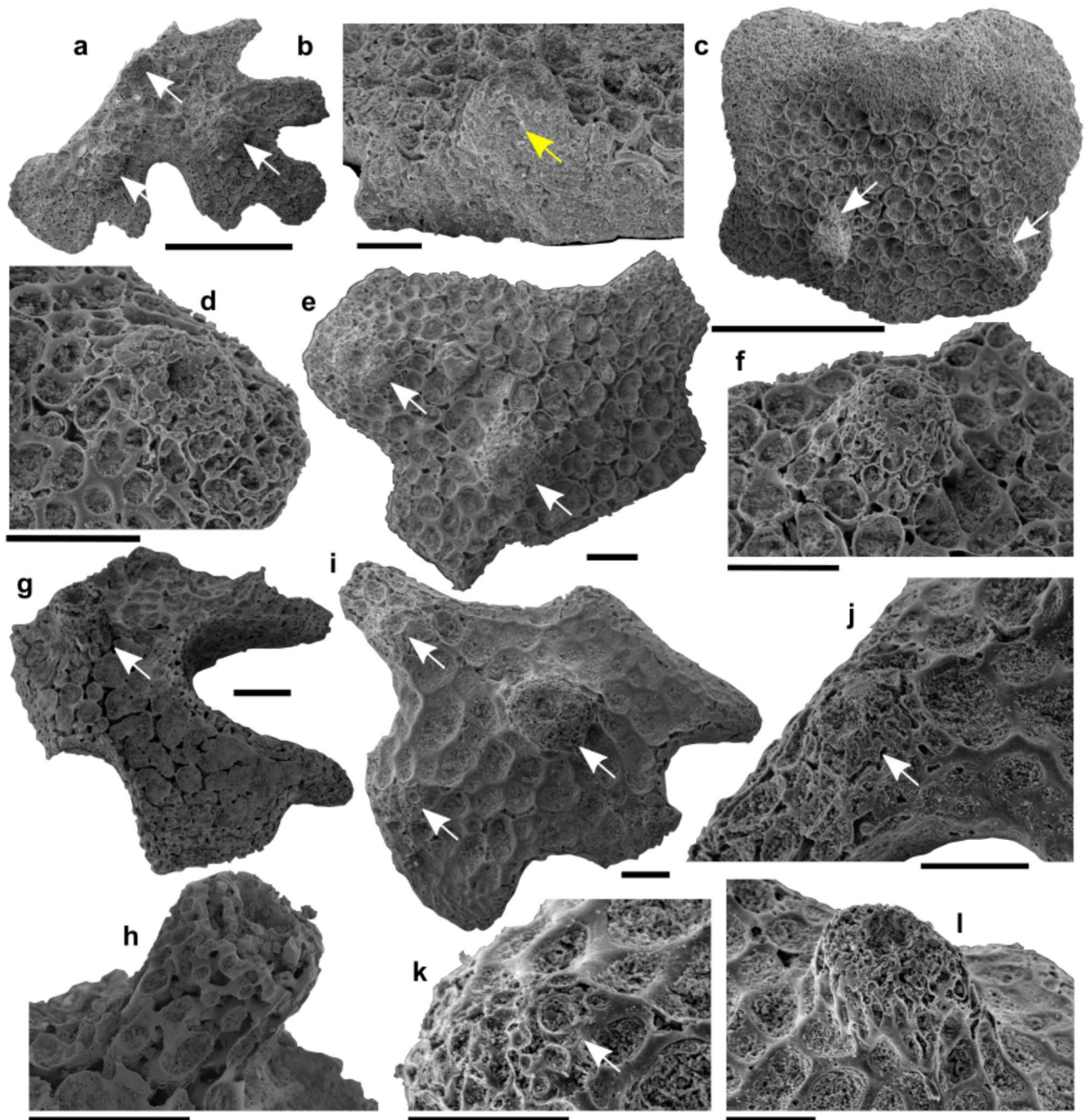


Fig. 2. Outgrowth structures on Cambrian disarticulated echinoderm plates of different size and shape. (a) Specimen USTL5297-5, plate fragment displaying three outgrowths, one being longitudinally sectioned at fragment edge. (b) Close-up on the cut outgrowth from specimen USTL5297-5. (c) Specimen USTL5297-11, plate with flat edge displaying two outgrowths of similar size and shape. (d–f) Specimen USTL5300-15, plate displaying two outgrowths of different size (close-up on each outgrowth in (d), (f)). (g–h) Specimen USTL5301-4, plate displaying one tall outgrowth, with a close-up (h). (i–l) specimen USTL5298-7, plate displaying three outgrowths of different size and shape, each outgrowth with a close-up (j–l). White arrows point to outgrowths. Yellow arrow points to pit within the outgrowth. Scale bars, 500 μm (a, c); 100 μm (c, d–j).

layer that tends to extend peripheral to and surrounding the outgrowth wall (Supplementary Fig. 6c), or (iii) at the surface of the external stereom layer (Supplementary Fig. 6b).

Discussion

One of the most distinctive features of both fossil and extant echinoderms is their mesh-like calcitic skeleton called stereom. The stereom microstructure has been shown to develop typical patterns depending on the echinoderm group, plate-type and, or location of the plate within the skeleton. Stereom has further been shown

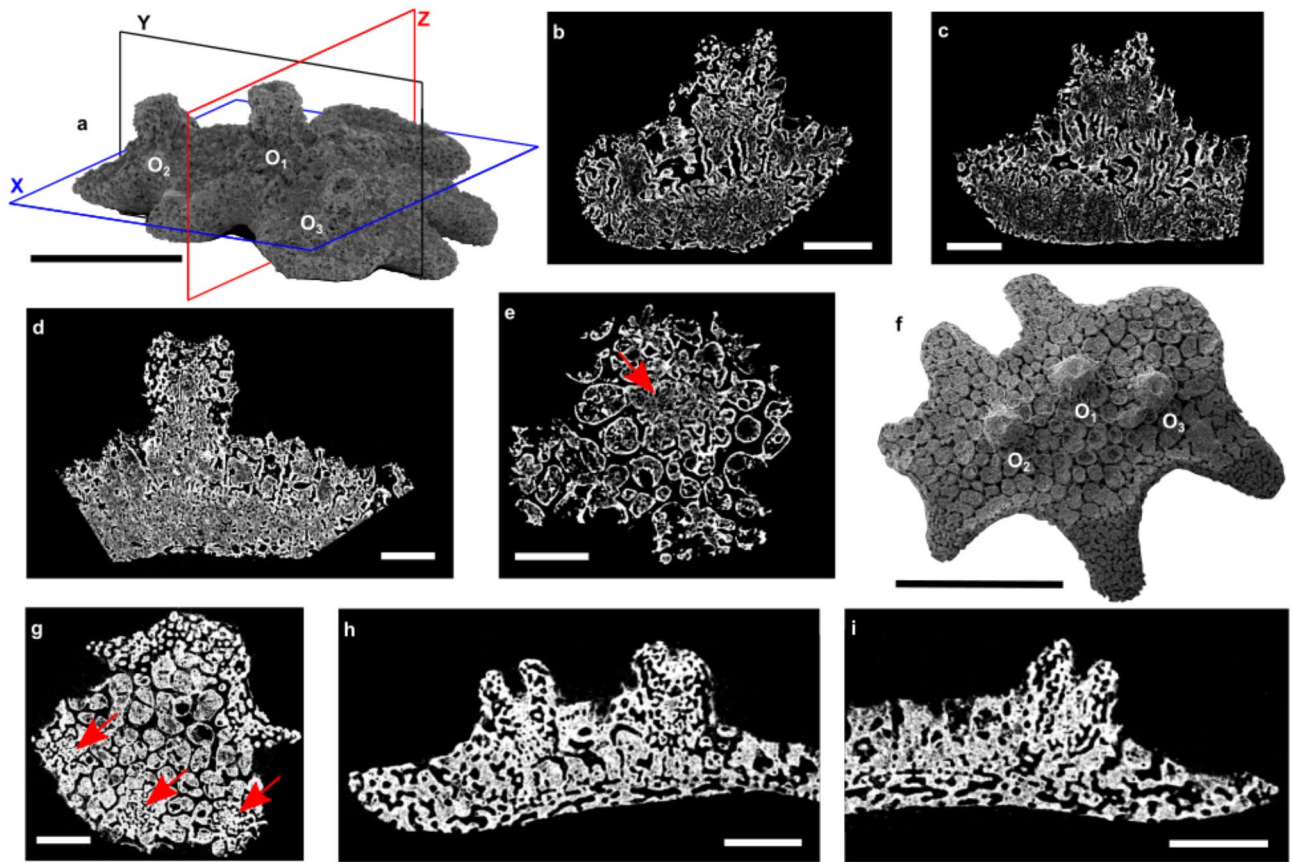


Fig. 3. CT-based 3D reconstruction of the internal microstructure of stereom showing microstructural difference between a plate and its associated outgrowths. **(a)** Specimen USTL5296, echinoderm plate displaying three outgrowths of different size (labelled O_1 , O_2 and O_3), with virtual orthogonal plans X, Y and Z. **(b)** Axial-section of O_2 according to plan Y. **(c)** Axial-section of O_3 according to plan Y. **(d)** Axial-section of O_1 according to plan Z. **(e)** Cross-section of O_1 at its base according to plan X, showing microstructural difference. **(f)** Specimen USTL5298-6 echinoderm plate displaying three outgrowths of different size. **(g)** Cross-sections of O_1 , O_2 and O_3 , at their base, according to plan X, showing microstructural difference. **(h)** Axial-section through the pit of O_2 and subaxial section of O_1 according to plan Y. **(i)** Axial-section of O_3 according to plan Y. Red arrows point to microstructural difference at the base of each outgrowth. O_1 = outgrowth 1; O_2 = outgrowth 2; O_3 = outgrowth 3. Scale bars, 500 μm (**a**, **e**); 50 μm (**b–d**, **f–h**).

to have a functional or mechanical significance and to even provide critical data on growth and associated soft tissue anatomy^{23,24}. As highlighted by Smith^{24,25}, considering one plate type, “the growth strategy adopted by a species is reflected in the plate construction (stereom) and it is therefore possible to identify the difference in emphasis placed on growth, reproduction, and maintenance”. Therefore, to identify growth irregularities in echinoderm plates, it is essential to examine their stereom microstructure.

Outgrowths presented in our study sometimes differ from the surrounding stereom of the echinoderm plate. This contrasts with ornamental structures, a feature frequently observed in Cambrian echinoderm plates, that do not differ from the plate stereom (see^{22,26}). Ornamental features in Cambrian plates typically manifest as mere plate thickenings and, moreover, lack a median pit—a characteristic present in all outgrowths documented in this study (Figs. 2 and 3 and Supplementary Figs. 1 and 2). These outgrowth characteristics are, therefore, not congruent with their interpretation as ornamental structures as seen in Cambrian plates. Modern asteroids, ophiuroids, and echinoids exhibit smaller ornamental features which stereom differs from underlying constitutive layers²⁷. These show a regular distribution on the plate surface with a constant structure and contact with underlying layers, differing with observed Cambrian outgrowths.

Pits are commonly observed on echinoderm functional tubercles (bearing or articulating with a spine). The oldest structures interpreted as thecal tubercles have been reported from Ordovician echinoderm plates attributed to the Class Echinoidea (sea urchins; see^{28–30}). Such tubercles have never been reported among Cambrian echinoderm representatives, despite their significant fossil record³¹. Tubercles in modern and fossil echinoids have a typical compact (imperforate to loosely microperforate) head, with a microperforate conical pit underneath permitting a ligamentous attachment with the spine²⁴. Although a ligamentary attachment within the described pit cannot be excluded, it cannot be deduced from the observed microstructure (absence of the typically associated stereom microstructures like e.g., microperforate or galleried stereom; Fig. 3). In addition, the outgrowths observed herein differ from functional tubercles, by clearly lacking an articulation surface

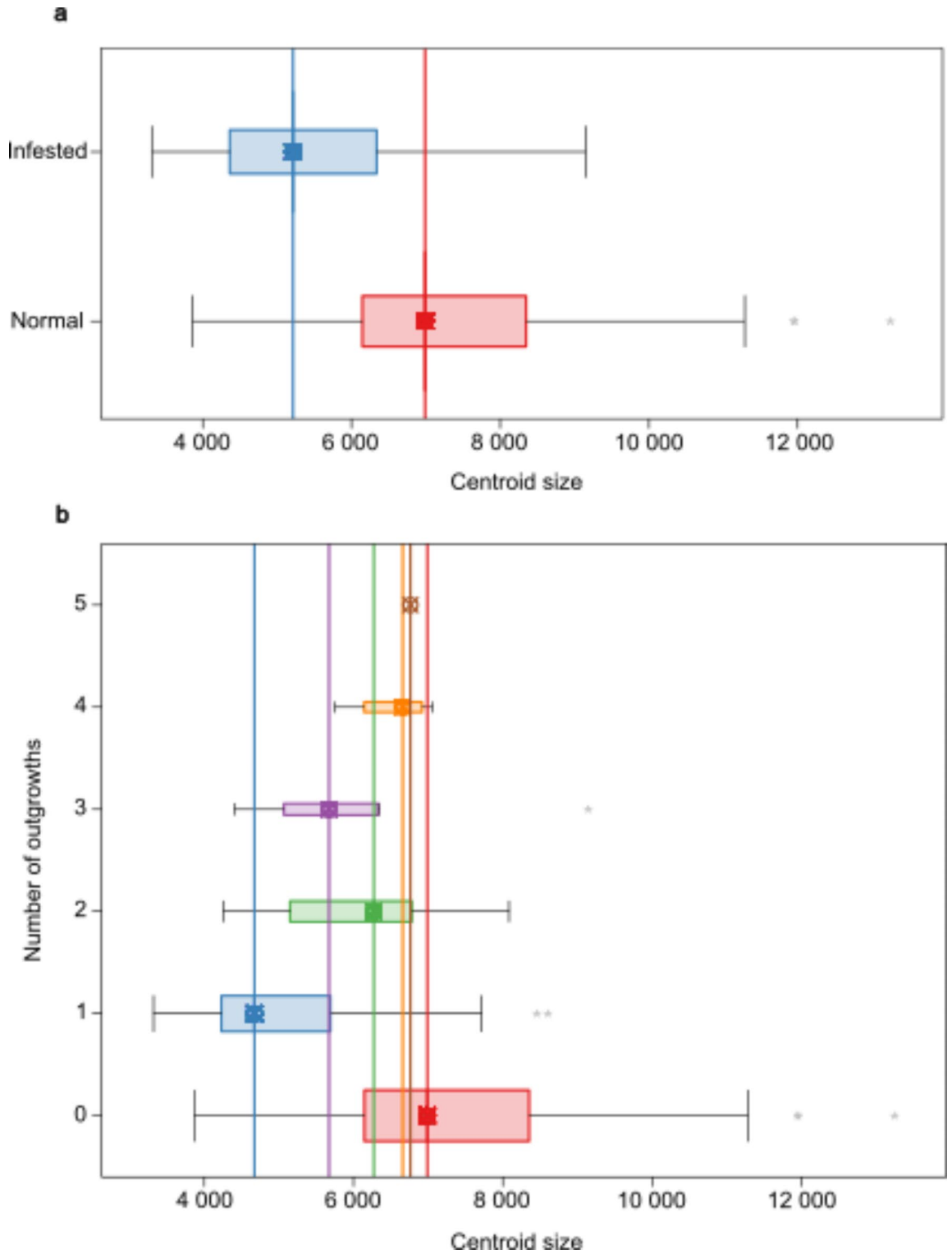


Fig. 4. Comparative distribution of centroid size among non-infested (“normal”) and infested echinoderm plates (a) and among the different number of outgrowths per plate (b). A box shows the interquartile range (IQR) of the distribution of a data subset and the whiskers the 1.5 IQR value. Vertical colored lines show the median centroid size for each subset.

covered by an imperforate to loosely microperforate stereom layer (Fig. 3 and Supplementary Figs. 2 and 6). The interpretation of observed outgrowth as ornamentation or functional tubercle is therefore precluded.

The lack of outgrowths on the internal surface of the recovered plates excludes the possibility of a post-mortem encrustation after the plates were disarticulated from each other and dispersed. Notwithstanding, the

low prevalence of the outgrowth-bearing plates within the assemblage, ca. 6% of epispire-bearing thecal plates, fulfills one of the parameters that are commonly pointed to in support to a “biotic interaction” interpretation³². In addition, among the 120 outgrowth-bearing plates, 31 plates exhibit two to five structures of variable dimensions (Supplementary Fig. 8). Such variably developed structures on a single plate, and secondarily between different plates, further suggests a progressive and relatively slow production of the structure by the echinoderms in response to a symbiont, its presence not immediately lethal to the host. Indeed, in echinoderms, growth deformities are considered to be produced by the echinoderm host while it was still alive and able to react to commensal or parasitic interactions³³. Conversely, these observations preclude a predatory interaction as: (i) predation is a short-term exploitative relationship eventually stimulating short term response (healing) from prey in case of rare abortive predation^{9,34} and (ii) predators most often kill their prey (preventing healing or reaction of the prey skeleton) whereas it is in the best interest of parasitic or commensal symbionts to keep their host alive.

The effect the interaction had on host and symbiont, whether positive, neutral or negative, is difficult to assess in the fossil record. Outgrowth-bearing plates like those documented here have never been reported from any articulated echinoderm specimens nor isolated ossicles known from more than 50 Cambrian echinoderm-bearing geological formations worldwide³¹. The lack of modern documented structures identical to the one described herein, also makes comparisons less straightforward. In the fossil record, interpreted parasitic interactions with an echinoderm as a host essentially consist of (i) the platyceratid-crinoid interaction¹⁵, in which the mollusk is directly attached to the echinoderm, with or without a skeletal reaction of the host; and (ii) galls or calluses on crinoid stems^{35,36}, where the size and shape of the callus and its genesis bear little resemblance to the outgrowths presented herein. There are however, structures such as *Phosphannulus*-type calluses or “bioclaustrations”³⁷ documented from other marine fossil phyla, that are surprisingly similar to the outgrowths reported herein. Bioclaustrations are generally characterized by a broad tubular morphology with a cylindrical opening at its distal end and have been described from Ordovician bryozoans^{37,38}, brachiopods³⁹, and Devonian corals⁴⁰. A similar morphology has also been reported on a stem of a crinoid from the Upper Jurassic⁴¹. Such a variety of hosts suggests that bioclaustrations correspond to a morphological reaction to a symbiont rather than a restricted relationship between two specific symbionts. Bioclaustrations have been interpreted as resulting from a parasitic³⁹ or commensal⁴⁰ relationship: the outgrowths are generated as a reaction to an invasive organism, the host progressively tending to repulse this organism from its skeletal surface, causing a disruption of epithelial secretion.

Bioclaustrations can result from endobiotic or epibiotic activity of the invasive symbiont. Endobiotic activity usually leads to a deep, internal skeletal perturbation associated with the bioclaustration outgrowth. CT cross-sections of infested plates from the middle Cambrian, Beetle Creek Formation show that their microstructure is variably perturbed surrounding the outgrowth (Fig. 3 and Supplementary Figs. 2 and 6). Based on comparisons with extant echinoderms^{24,25}, the construction and thickness of the constitutive layers are thought to reflect the growth of the thecal plates. Consequently, the internal perturbations in the stereom, observed at different constitutive layers following the formation of outgrowths, are here interpreted as the result of epibiont attachment at various growth stages of the echinoderm plates. In our study, because the outgrowths only occur on the external plate surface with no selectivity regarding plate-shape (Supplementary Fig. 7), it is most likely that the echinoderm host primarily represented an attachment surface, potentially essential for the epibiont to survive and grow. Recorded perturbation and repulsion suggest a reaction to a threat, and the energetic cost provided in such response is considered more detrimental than beneficial to the host.

Even if there is no clear relationship between the size of a plate and the number of outgrowths it develops, infested plates are shown to be significantly reduced in size compared with uninfested plates (Fig. 4a). Such a reduction in host size, or at least evidence of growth retardation indicates a detrimental effect on the host⁴². Comparing the effects on growth in infested versus uninfested host specimens in large sample sizes allows us to constrain the nature of interactions⁴³ without relying on phylogenetic conservativeness. Considering the significant reduction in plate-size of infested echinoderm plates, our analyses reveal that the epibiont might have directly affected the biological fitness of the echinoderm host, providing strong evidence that these epibionts were parasitic rather than mutualistic or commensal with their echinoderm hosts. Similar reductions in host biomass or growth rates have been widely documented in modern parasitic relationships, where parasites increase the host’s energetic demands as they must not only meet their own energy needs but also sustain those of the parasite, often resulting in decreased size compared to uninfected individuals. Such an effect has rarely been reported in the fossil record¹⁴, as several infested and normal (uninfested) hosts need to be found in the same assemblage, to make a robust comparison of size and growth. However, even if the recovered assemblage is large, our analysis considers the measurement of individual echinoderm plates rather than the entire body size of the organism, so that this result should be considered with caution.

All infested plates are epispire-bearing plates, hence they most probably belonged to a blastozoan or an edrioasteroid echinoderm, although a stylophoran affinity cannot be definitely rejected. Among the studied assemblage, edrioasteroid or blastozoan specific plates, such as ambulacral or brachiolar plates, have been reported but never observed with outgrowths, precluding any further systematic assignment. Although our analyses indicate that the outgrowths are a reaction to parasitic epibionts, the deduced epibiont is, most likely due to taphonomic reasons, never preserved associated with the reported outgrowths. Even if the identity and ecology of the epibiont would be required to definitely establish that the observed structures are resulting from a parasitic interaction, it is important to note that the vast majority of parasites deduced from the fossil record remain unknown⁶. Bioclaustrations, the morphological perturbation that most closely resembles the outgrowths presented herein, have been interpreted to be generated by suspension-feeding tube-dwelling animals, a suggestion that seems plausible according to the Cambrian record. Tube-dwelling organisms have already been shown to have encrusted sessile creatures in enduring parasitic relationships in the Cambrian¹⁴. In this

instance, the tube-dwelling organisms were interpreted as kleptoparasites, stealing the food that the brachiopod host had expended energy on obtaining and capturing¹⁴. Even if the edrioasteroids and blastozoans, sessile suspension-feeder animals, have been recognized as potential hosts involved in the interaction described herein, a kleptoparasitic relationship cannot be assessed without further identification of the parasitic epibiont. The diameter (20–70 μm) and length (40–210 μm) of the outgrowth pit may to some extent reflect the measurements of the associated epibiont, whereas the total diameter of the outgrowth (> 70 μm ; Supplementary Figs. 3–5) would be originally controlled by the host. However, as a potential suspension-feeder, the epibiont may have had an everted anterior body-part that exceeded the extremity of the outgrowth, limiting our ability to accurately estimate the size of the epibiont.

Echinoderms throughout the Phanerozoic have greatly increased our knowledge of parasitism⁴⁴. Various responses to parasitism have been documented across fossil echinoderm assemblages^{15,35,36,45–47}, but the outgrowths documented here are unique. The variable dimensions and distribution of outgrowths on the external plate surface, their microstructure, their variable settlement in relation with the plate constitutive layers (among and within plates), along with the size reduction of infested plates, are all lines of evidence that support the interpretation that these outgrowths on middle Cambrian echinoderms are a reaction to biotic interactions. The outgrowths described in this study not only represent a new type of morphological reaction in extinct echinoderm classes to epibionts but also mark the oldest evidence of parasitic symbiotic interactions on echinoderm hosts. This finding provides further evidence that parasite-host interactions were already well-established and widespread across many phyla heading into the Wuliuan Stage of the Cambrian, emphasizing the Cambrian as a critical period of ecological innovation and diversification.

Methods

Material

All studied echinoderm plates were collected from middle Cambrian rocks of the Burke River Structural Belt in the sedimentary Duchess Embayment sub-basin in the eastern part of the Georgina Basin, Queensland, Australia (Fig. 1). The Georgina Basin covers a surface of 325 000 km^2 , shared by Queensland and Northern Territory in Australia. In the Duchess Embayment area, the sedimentary succession has been divided into four major lithological units: the Mount Birnie Beds (sandstone-conglomerate), the Thornton Limestone Formation (organic-rich dolomite), the Beetle Creek Formation (chert-siltstone to limestone-phosphorite) and Inca Formation (silt-chertshale). According to previous works^{48,49}, the first two formations represent a first slow transgressive system tract. Following a regression, the Beetle Creek and Inca formations correspond to a second transgressive system tract during a new deepening sequence. The Beetle Creek Formation is divided into a lower organic rich phosphatic facies, either considered as deposited in areas of restricted circulation, or a relatively deep-water setting, and an upper Monastery Creek Phosphorite Member ending at a concretionary limestone layer, interpreted as a condensed section²¹. All echinoderm plates come from one of the phosphatic, bioclast-rich limestones within the Monastery Creek Phosphorite Member. This calcareous facies has yielded a rich and diverse fauna²¹. This faunal assemblage belongs to the *Triplagnostus gibbus*/*Acidusus atavus* zones and is late Templetonian/early Florian in age according to the Australian correlation chart of Gravestock and Shergold⁴⁸, corresponding to the Wuliuan Stage of the International Chart. Unfortunately, no articulated echinoderm specimens were recovered from the Monastery Creek Phosphorite Member and only isolated plates or fragments have been extracted. Along with the isolated plate material described herein, isolated echinoderm fragments of pelmatozoan ossicles, *Stromatocystites* ambulacral ossicles, indeterminate epispire-bearing thecal plates, and stylophoran appendage ossicles have been identified²¹. With the exception of a dozen ossicles, all thecal plates targeted here are complete. The calcitic stereom of studied ossicles has been phosphatized (as detailed in²¹). The quality of preservation varies but allows key measurements to be done, most of the time. Limestone samples were etched with a 10% acetic acid solution. Residues were sieved using 1 mm and 200 μm meshes before being sorted under binocular microscope and prepared for scanning electron microscopy observation. The material is stored at the University of Lille, France (USTL collection numbers).

Data imaging

Studied fossils are microscopic skeletal elements of echinoderms, therefore 2D and 3D appropriate imaging techniques have been used to further investigate these fossils qualitatively and quantitatively. Specimens are placed on a carbon tape and are gold coated, then analyzed with a ZEISS 'EVO' Scanning Electron Microscope (SEM) housed at the University of Lille, France, using an accelerating voltage of 15 kV, in order to acquire precise 2D pictures of them (Fig. 2 and Supplementary Fig. 1).

3D microstructure of the plates and outgrowths was acquired and reconstructed through micro-computed tomographic approaches. Two plates (specimen USTL5294 and specimen USTL5295, respectively represented in Supplementary Fig. 2a–b and Supplementary Fig. 2c–e) were analyzed at an energy level of 17.6 keV (voxel size = 0.678 μm) and one (specimen USTL5296, represented in Fig. 3a–e) was at 30 keV (voxel size = 0.75 μm) with the synchrotron X-ray μ -tomography of the European Synchrotron Radiation Facility (ESRF) in Grenoble, France. Depending on their size between 1642 and 2049 projections were taken. The reconstructions resulted in stacks of 16-bit TIF images. Four plates (specimens USTL5298-6, USTL5298-7, USTL5300-15, and USTL5302-6) were scanned at Ghent University using Nanowood⁵⁰, using the setup with the open-type Hamamatsu transmission tube and the large-area Varian detector. The plates were scanned at 80 kV and 4 W using no additional filter. Depending on their size between 1401 and 1901 projections were taken, using an exposure time of 1.5 s per projection. Each projection consisted of two averages. The total scan time ranged between 78 and 103 min. All scans were reconstructed with Octopus reconstruction version 8.9.4.9 (XRE) using the in-house protocol. Spot, noise and ring filtering were applied, and movement and beam hardening corrections were performed. The reconstructions resulted in stacks of 16-bit TIF images representing the scanned volumes

with a voxel size of either 0.9–1.0 μm . These scanned imaging voxel data were segmented and tessellated with the software AVIZO (Fire Edition 8.0.0). Based on these 3D reconstructions, 2D slices were made following the three major axes of the plate to inspect the internal microstructure of the plates and their outgrowths (Fig. 3 and Supplementary Fig. 2). Stereom coarseness (trabeculae and pore thicknesses) was measured using the 2D slices.

Morphometric analyses

To evaluate the possible impact of outgrowths on their bearing plates compared to uninfested plates, several morphometric analyses were carried out. First, studied echinoderm plates are classified according to their number of outgrowths and compared to a series of plates devoid of such outgrowths (Supplementary Fig. 7). Second, outgrowths and plates are described by classical linear morphometrics with the following measurements: maximum length of a plate, height and basal diameter of an outgrowth, and diameter of an outgrowth pit / aperture. To reduce 'error measurement', each parameter is acquired five times before recording the mean value rounded to the closest integer at a μm scale. In total, 99 outgrowths from 65 complete or fragmentary plates have been quantified with this approach. Additional material (infested and non-infested plates) was sorted from residues and remains available for further analyses. Then, the distribution of these measurements among their range classes and according to the number of outgrowths is explored for each parameter (Supplementary Figs. 3–5). Last, covariation among these measurements is tested by means of the Pearson's correlation coefficient (Supplementary Fig. 7). Third, the shape of complete plates, with or without outgrowths, is quantified by modern geometric morphometrics⁵¹: (i) the outline of 74 complete plates (some complete plates were utilized for geometric morphometrics and not for linear morphometrics, and vice-versa) bearing outgrowths and 98 without outgrowths have been digitized each by a series of 250 equally-spaced semilandmarks⁵²; (ii) then, the digitized plates are standardized by rescaling them to unit centroid size, translating them to their centroid, and rotating them along their major axis of elongation; (iii) next, the superimposed outlines are modeled each by an elliptical Fourier analysis^{53–55} with 11 harmonics, which encompass 99% of the total harmonic power; (iv) finally the harmonic coefficients are ordinated by a centred and unscaled principal component analysis to create a multidimensional morphological space⁵⁶, which can be used to explore the morphological variability among studied plates, notably if the presence/absence of outgrowths is linked to peculiar shapes (Supplementary Fig. 7). Fourth, the possible relationship of outgrowths with the 'size' of plates is evaluated by comparing the distribution of their centroid size⁵⁷ (see Fig. 4). Finally, during the semilandmark digitizing, the position of each outgrowth has also been marked by a fake landmark at its basal center (not included in the geometric morphometric analysis above). This position of outgrowths is then used to compute their minimal distance from their plate's border and their distance from their plate's center (Supplementary Fig. 9).

Morphometric and statistical analyses are computed using R (version 4.1.3⁵⁶) and the packages 'geomorph' (v. 4.0.3⁵⁹), 'Momocs' (v. 1.4.1⁵⁵) and 'sf' (v. 1.0.8⁶⁰), and landmarks of outgrowths and semilandmarks of plates' outlines are digitized using the software TPSdig (v. 2.32^{61,62}).

Data availability

All data generated or analyzed is provided within this manuscript or in supplementary information files. The CT datasets studied in this work can be found online, on the YODA repository of Utrecht University: <https://doi.org/10.24416/UU01-2ADPCS>.

Received: 31 January 2025; Accepted: 8 April 2025

Published online: 24 April 2025

References

- Bambach, R. K., Bush, A. M. & Erwin, D. H. Autecology and the filling of ecospace: Key metazoan radiations. *Palaeontology* **50**(1), 1–22. <https://doi.org/10.1111/j.1475-4983.2006.00611.x> (2007).
- Novack-Gottshall, P. M. Using a theoretical ecospace to quantify the ecological diversity of Paleozoic and modern marine biotas. *Paleobiology* **33**(2), 273–294. <https://doi.org/10.1666/06054.1> (2007).
- Bush, A. M., Bambach, R. K. & Erwin, D. H. Ecospace utilization during the Ediacaran radiation and the Cambrian eco-explosion. *Quantifying Evol. Early Life: Numer. Approaches Evaluation Fossils Anc. Ecosyst.* 111–133. https://doi.org/10.1007/978-94-007-0680-4_5 (2011).
- Klompaker, A. A. & Boxshall, G. A. Fossil crustaceans as parasites and hosts. *Adv. Parasitol.* **90**, 233–289. <https://doi.org/10.1016/bs.apar.2015.06.001> (2015).
- Klompaker, A. A. et al. M. Predation in the marine fossil record: Studies, data, recognition, environmental factors, and behavior. *Earth-Sci. Rev.* **194**, 472–520. <https://doi.org/10.1016/j.earscirev.2019.02.020> (2019).
- De Baets, K., Huntley, J. W., Scarponi, D., Klompaker, A. A. & Skawina, A. Phanerozoic parasitism and marine metazoan diversity: Dilution versus amplification. *Philosophical Trans. Royal Soc. B* **376**(1837), 20200366. <https://doi.org/10.1098/rstb.2020.0366> (2021).
- De Baets, K., Huntley, J. W., Klompaker, A. A., Schiffbauer, J. D. & Muscente, A. D. The fossil record of parasitism: its extent and taphonomic constraints. *Evol. Fossil Record Parasitism: Coevol. Paleoparasitological Techniques.* 1–50. https://doi.org/10.1007/978-3-030-52233-9_1 (2021).
- Vinn, O. Early symbiotic interactions in the cambrian. *Palaios* **32**(4), 231–237. <https://doi.org/10.2110/palo.2016.092> (2017).
- Vinn, O. Traces of predation in the cambrian. *Hist. Biol.* **30**(8), 1043–1049. <https://doi.org/10.1080/08912963.2017.1329305> (2018).
- Nanglu, K. & B Caron, J. Symbiosis in the cambrian: Enteropneust tubes from the Burgess shale co-inhabited by commensal polychaetes. *Proc. R Soc. B.* **288**, 20210061. <https://doi.org/10.1098/rspb.2021.0061> (2021).
- Topper, T. P., Holmer, L. E. & Caron, J. B. Brachiopods hitching a ride: An early case of commensalism in the middle cambrian Burgess shale. *Sci. Rep.* **4**(1), 6704. <https://doi.org/10.1038/srep06704> (2014).
- Topper, T. P. Competition and mimicry: The curious case of Chaetae in brachiopods from the middle cambrian Burgess shale. *BMC Evol. Biol.* **15**, 42. <https://doi.org/10.1186/s12862-015-0314-4> (2015).
- Bassett, M. G., Popov, L. E. & Holmer, L. E. The oldest-known metazoan parasite? *J. Paleontol.* **78**(6), 1214–1216. [https://doi.org/10.1666/0022-3360\(2004\)078<1214:TOMP>2.0.CO;2](https://doi.org/10.1666/0022-3360(2004)078<1214:TOMP>2.0.CO;2) (2004).

14. Zhang, Z. et al. An encrusting kleptoparasite-host interaction from the early cambrian. *Nat. Commun.* **11** (1), 2625. <https://doi.org/10.1038/s41467-020-16332-3> (2020).
15. Baumiller, T. K. & Gahn, F. J. Fossil record of parasitism on marine invertebrates with special emphasis on the platyceratid-crinoid interaction. *Pal Soc. Papers.* **8**, 195–210. <https://doi.org/10.1017/S108933260001091> (2002).
16. Caron, J. B. & Jackson, D. A. Paleoeology of the greater phyllopod bed community, Burgess shale. *Palaeogeogr Palaeoclim Palaeoeco* **258**(3), 222–256. <https://doi.org/10.1016/j.palaeo.2007.05.023> (2008).
17. Paterson, J. R. The Emu Bay shale Konservat-Lagerstätte: A view of cambrian life from East Gondwana. *J. Geol. Soc.* **173**(1), 1–11. <https://doi.org/10.1144/jgs2015-083> (2016).
18. Xian-Guang, H. et al. The Cambrian fossils of Chengjiang, China: the flowering of early animal life. *John Wiley and Sons* (2017).
19. Harper, D. A. et al. M. P. The Sirius passet lagerstätte of North Greenland: A remote window on the cambrian explosion. *J. Geol. Soc.* **176**(6), 1023–1037. <https://doi.org/10.1144/jgs2019-043> (2019).
20. Deline, B. The first evidence of predatory or parasitic drilling in stylophoran echinoderms. *Acta Palaeontol. Pol.* **53**(4), 739–743 (2008).
21. Clausen, S., Jell, P. A., Legrain, X. & Smith, A. B. Pelmatozoan arms from the middle cambrian of Australia: Bridging the gap between brachioles and brachials? *Lethaia* **42**(3), 283–296. <https://doi.org/10.1111/j.1502-3931.2008.00145.x> (2009).
22. Clausen, S. & Peel, J. S. Middle cambrian echinoderm remains from the Henson Gletscher formation of North Greenland. *GFF* **134**(3), 173–200. <https://doi.org/10.1080/11035897.2012.721003> (2012).
23. Macurda, D. B. & Meyer, D. L. The microstructure of the crinoid endoskeleton. *Paleontological Contribution Univ. Kans.* **74**, 1–22 (1975).
24. Smith, A. B. Stereom microstructure of the echinoid test. *Spec. Papers Palaeont* **25**, 1–81 (1980).
25. Smith, A. B. Biomineralization in echinoderms. In (ed Carter, J. G.) *Skeletal Biomineralization: Patterns, Processes, and Evolutionary Trends* 413–443. Van Nostrand Reinhold, New York. (1990).
26. Guensburg, T. E. & Sprinkle, J. Revised phylogeny and functional interpretation of the Edrioasteroidea based on new taxa from the early and middle ordovician of Western Utah. *Fieldiana Geol.* **29**, 1–41 (1994).
27. Gorzelak, P., Torres Jr, L., Kolbuk, D., Grun, T. B. & Kowalewski, M. Geochemical signatures and Nanomechanical properties of echinoid tests from nearshore habitats of Florida: Environmental and physiological controls on echinoid biomineralization. *PeerJ* **13**, e18688 (2025).
28. Pisera, A. Echinoderms of the Mójca limestone. *Palaeontol. Pol.* **53**, 283–307 (1994).
29. Thompson, J. R. et al. The ordovician diversification of sea urchins: Systematics of the Bothriocidaroida (Echinodermata: Echinoidea). *J. Syst. Palaeontol.* **19**(20), 1395–1448. <https://doi.org/10.1080/14772019.2022.2042408> (2022).
30. Jell, P. A. & Theron, J. N. Early devonian echinoderms from South Africa. *Mem. Qld. Museum* **43**, 115–199 (1999).
31. Zamora, S. et al. Chapter 13 cambrian echinoderm diversity and palaeobiogeography. *Geol. Soc. Lond. Mem.* **38**(1), 157–171. <https://doi.org/10.1144/M38.13> (2013).
32. De Baets, K., Klug, C. & Korn, D. Devonian pearls and ammonoid – endoparasite co – evolution. *Acta Palaeontol. Pol.* **56**(1), 159–180. <https://doi.org/10.4202/app.2010.0044> (2011).
33. Donovan, S. K. A prejudiced review of ancient parasites and their host echinoderms: CSI fossil record or just an excuse for speculation? *Adv. Parasitol.* **90**, 291–328. <https://doi.org/10.1016/bs.apar.2015.05.003> (2015).
34. Conway Morris, S. & Bengtson, S. Cambrian predators: Possible evidence from boreholes. *J. Paleontol.* **68**(1), 1–23 (1994).
35. Welch, J. R. *Phosphannulus* on paleozoic crinoid stems. *J. Paleontol.* 218–225 (1976).
36. Radwańska, U. & Radwański, A. Myzostomid and copepod infestation of jurassic echinoderms: A general approach, some new occurrences, and/or re-interpretation of previous reports. *Acta Geol. Pol.* **55**(2), 109–130 (2005).
37. Vinn, O., Ernst, A. & Toom, U. Bioclustrations in upper ordovician bryozoans from Northern Estonia. *Neues Jahrbuch Für Geologie Und Paläontologie-Abhandlungen* 113–121. <https://doi.org/10.1127/njgpa/2018/0752> (2018).
38. Vinn, O., Ernst, A., Wilson, M. A. & Toom, U. Symbiosis in Trepostome bryozoans from the sandbian (Late Ordovician) of Estonia. *Hist. Biol.* **34**(6), 1029–1038. <https://doi.org/10.1080/08912963.2021.1959579> (2022).
39. Vinn, O., Wilson, M. A. & Toom, U. Earliest rhychonelliform brachiopod parasite from the late ordovician of Northern Estonia (Baltica). *Palaeogeogr Palaeoclim Palaeoeco* **411**, 42–45. <https://doi.org/10.1016/j.palaeo.2014.06.028> (2014).
40. Zatoń, M. & Wrzolek, T. Colonization of rugose corals by diverse epibionts: Dominance and syn vivo encrustation in a middle devonian (Givetian) soft-bottom habitat of the holy cross mountains, Poland. *Palaeogeogr Palaeoclim Palaeoeco.* **556**, 109899. <https://doi.org/10.1016/j.palaeo.2020.109899> (2020).
41. Zamora, S. & Systematics Taphonomy, and Paleoeology of Millericrinids (Millericrinida, Articulata, Crinoidea) from the Late Jurassic of Spain. *Contributions: Museum of Paleontology, University of Michigan* **34**(7), 82–102. <https://doi.org/10.7302/4251> (2022).
42. Gahn, F. J. & Baumiller, T. K. Infestation of middle devonian (Givetian) camerate crinoids by platyceratid gastropods and its implications for the nature of their biotic interaction. *Lethaia* **36**(2), 71–82. <https://doi.org/10.1080/00241160310003072> (2003).
43. Baumiller, T. K. Evaluating the interaction between platyceratid gastropods and crinoids: A cost–benefit approach. *Palaeogeogr Palaeoclim Palaeoeco.* **201**(3–4), 199–209 (2003).
44. Smith, A. B., Zamora, S. & Álvaro, J. J. The oldest echinoderm faunas from Gondwana show that echinoderm body plan diversification was rapid. *Nat. Commun.* **4**(1), 1385. <https://doi.org/10.1038/ncomms2391> (2013).
45. Thomka, J. R. & Brett, C. E. Parasitism of paleozoic crinoids and related stalked echinoderms: paleopathology, ichnology, Coevolution, and evolutionary paleoeology. *Evol. Fossil Record Parasitism: Coevol. Paleoparasitological Techniques.* 289–316. https://doi.org/10.1007/978-3-030-52233-9_9 (2021).
46. Brett, C. E. *Tremichnus*: a new ichnogenus of circular-parabolic pits in fossil echinoderms. *J. Paleontol.* 625–635 (1985).
47. Farrar, L. et al. Characterization of traces of predation and parasitism on fossil echinoids. *Palaios* **35**(5), 215–227. <https://doi.org/10.2110/palo.2019.088> (2020).
48. Southgate, P. N. & Shergold, J. H. Application of sequence stratigraphic concepts to middle cambrian phosphogenesis, Georgina basin, Australia. *Bureau Mineral. Ressource J. Australian Geol. Geophys.* **12**, 119–144 (1991).
49. Gravestock, D. I. & Shergold, J. H. Australian early and middle cambrian sequence biostratigraphy with implications for species diversity and correlation. In (eds Zhuravlev, A. Y. & Riding, R.) *The Ecology of the Cambrian Radiation* 107–136. Columbia University, New York. <https://doi.org/10.7312/zhur10612-006> (2001).
50. Dierick, M. et al. Recent micro-CT scanner developments at UGCT. *Nucl. Instrum. Methods Phys. Res., Sect. B* **324**, 35–40 (2014).
51. Zelditch, M. L., Swiderski, D. L. & Sheets, H. D. Geometric morphometrics for biologists: A primer. Second edition. Academic Press, 488 pp. (2012).
52. Gunz, P., Mitteroecker, P. & Semilandmarks A method for quantifying curves and surfaces. *Hystrix* **24**, 103–109. <https://doi.org/10.4404/hystrix-24.1-6292> (2013).
53. Kuhl, F. P. & Giardina, C. R. Elliptic fourier features of a closed contour. *Comput. Graphics Image Process.* **18**, 236–258. [https://doi.org/10.1016/0146-664X\(82\)90034-X](https://doi.org/10.1016/0146-664X(82)90034-X) (1982).
54. Haines, A. J. & Crompton, J. S. Improvements to the method of fourier shape analysis as applied in morphometric studies. *Palaeontology* **43**, 765–783. <https://doi.org/10.1111/1475-4983.00148> (2000).
55. Bonhomme, V., Picq, S., Gaucherel, C., Claude, J. & Momocs Outline analysis using R. *J. Stat. Softw.* **56**, 1–24. <https://doi.org/10.18637/jss.v056.i13> (2014).
56. Budd, G. E. & Morphospace *Curr. Biol.* **31**(19), R1181–R1185. doi: <https://doi.org/10.1016/j.cub.2021.08.040> (2021).

57. Klingenberg, C. P. Size, shape, and form: concepts of allometry in geometric morphometrics. *Dev. Genes Evol.* **226**, 113–137. <https://doi.org/10.1007/s00427-016-0539-2> (2016).
58. R Core Team. R: A language and environment for statistical computing. R Foundation for Statistical Computing, Vienna, Austria, (2022). <https://www.R-project.org/>
59. Baken, E. K., Collyer, M. L., Kaliontzopoulou, A. & Adams, D. C. Geomorph v4.0 and GmShiny: enhanced analytics and a new graphical interface for a comprehensive morphometric experience. *Methods Ecol. Evol.* **12**, 2355–2363. <https://doi.org/10.1111/2041-210X.13723> (2021).
60. Pebesma, E. & Bivand, R. Spatial Data Science: With Applications in R. Chapman and Hall/CRC. <https://doi.org/10.1201/9780429459016> (2023).
61. Rohlf, F. J. *Tps Utility Program, Ver. 1.50. Department of Ecology and Evolution, Stony Brook* (State University of New York, 2012).
62. Rohlf, F. J. The Tps series of software. *Hystrix* **26**, 9–12. <https://doi.org/10.4404/hystrix-26.1-11264> (2015).

Acknowledgements

This project has received funding from the European Union's Horizon 2020 research and innovation programme under grant agreement No 101005611 for Transnational Access conducted at Ghent University. The Ghent University Special Research Fund (BOF-UGent) is acknowledged to support the UGent Core facility UGCT (BOF/COR/2022/008). K.D.B. was supported by the I.3.4 Action of the Excellence Initiative - Research University Programme at the University of Warsaw (Project: PARADIVE). Financial support from Vetenskraprådet (VR-2021-04295) and National Science Foundation of China (42072003) is acknowledged by T.P.T. We would like to thank the staff of the ESRF and EMBL Grenoble for assistance and support in using beamline(s) ID19 under proposal number EC-686. We thank Samuel Zamora, William I. Ausich, and Editor Przemysław Gorzelak for making constructive comments.

Author contributions

I.G. and S.C. designed the study. K.D.B. made several suggestions on quantitative analyses to pursue. P.A.J. and S.C. did the fieldwork and collected the material. I.G. did the measurements. I.G. and S.R. took SEM pictures. L.S., V.C. and S.C. collected X-ray data. L.S., V.C. and I.G. treated X-ray data. I.G. and C.M. did statistical and quantitative analyses. I.G., S.C., T.P.T. and C.M. wrote the manuscript, with input from K.D.B. and L.S. All authors discussed and agreed on interpretation of the data.

Declarations

Competing interests

The authors declare no competing interests.

Additional information

Supplementary Information The online version contains supplementary material available at <https://doi.org/10.1038/s41598-025-97932-1>.

Correspondence and requests for materials should be addressed to I.G.

Reprints and permissions information is available at www.nature.com/reprints.

Publisher's note Springer Nature remains neutral with regard to jurisdictional claims in published maps and institutional affiliations.

Open Access This article is licensed under a Creative Commons Attribution-NonCommercial-NoDerivatives 4.0 International License, which permits any non-commercial use, sharing, distribution and reproduction in any medium or format, as long as you give appropriate credit to the original author(s) and the source, provide a link to the Creative Commons licence, and indicate if you modified the licensed material. You do not have permission under this licence to share adapted material derived from this article or parts of it. The images or other third party material in this article are included in the article's Creative Commons licence, unless indicated otherwise in a credit line to the material. If material is not included in the article's Creative Commons licence and your intended use is not permitted by statutory regulation or exceeds the permitted use, you will need to obtain permission directly from the copyright holder. To view a copy of this licence, visit <http://creativecommons.org/licenses/by-nc-nd/4.0/>.

© The Author(s) 2025